Engineering Structures 41 (2012) 242–257

Contents lists available at SciVerse ScienceDirect

Engineering Structures

journal homepage: www.elsevier.com/locate/engstruct

Semi-active fuzzy control of a wind-excited tall building using multi-objective genetic algorithm

Hyun-Su Kim [a], Joo-Won Kang [b,*]

[a] Division of Architecture, Sunmoon University, Asan-si, Republic of Korea
[b] School of Architecture, Yeungnam University, Gyeongsan-si, Republic of Korea

ARTICLE INFO

Article history:
Received 7 July 2011
Revised 19 March 2012
Accepted 21 March 2012
Available online 28 April 2012

Keywords:
Multi-objective genetic algorithms
Wind-induced response control
Semi-active tuned mass damper
MR damper
Fuzzy logic control system
Tall building

ABSTRACT

In this study, a multi-objective optimal fuzzy control system for the response reduction of a wind-excited tall building has been proposed. A semi-active tuned mass damper (STMD) is used for vibration control of a 76-story benchmark building subjected to wind load. An STMD consists of a 100 kN magnetorheological (MR) damper and its natural period is tuned to the first-mode natural period of vibration of the example building structure. The damping force of the MR damper is controlled by a fuzzy logic controller. A multi-objective genetic algorithm is used for optimization of the fuzzy logic controller. Both the 75th floor acceleration response of the structure and the stroke of the STMD have been used as the objective functions for this multi-objective optimization problem. Because a multi-objective optimization approach provides a set of Pareto-optimal solutions, an engineer is able to select an appropriate design for the specific performance requirement. For a comparative study, a sky–ground hook control algorithm is employed for control of the STMD. Based on numerical results, it has been shown that the proposed control system can effectively reduce the STMD motion as well as building responses compared to the comparative sky–ground hook control algorithm. In addition, the control performance of the STMD controlled by the optimal fuzzy controller is superior to that of the passive TMD and is comparable to an active TMD, but with a significant reduction in power consumption.

1. Introduction

One of the challenging tasks for structural engineers is to mitigate the dynamic responses of a tall building structure subjected to wind loads in order to prevent human discomfort and motion sickness, and sometimes to enhance structural safety and integrity. Over the past decades, structural control methods have shown great potential to reduce the wind-excited vibration of tall building structures. The tuned mass damper (TMD) is one of the most widely used and accepted wind response control systems for tall buildings. Conventional passive TMD, which requires no external power, is reliable and does not destabilize the structure. However, the very narrow band of suppression frequency, the ineffective reduction of non-stationary vibrations, and the sensitivity problems due to mistuning are the inherent limitations of a conventional TMD [1,2]. In order to enhance the control performance of a TMD, an active force used to act between the structure and the TMD is introduced, that is an active TMD (ATMD) [3,4]. However, its stability problems, reliability and large power consumption are still major concerns to engineers. As a response to this, semi-active control devices are presented, which utilize the performance benefits while seeking to remedy the lack of stability of active systems. These devices only absorb or store the vibratory energy and they do not input the energy to the system. Therefore, they do not induce adverse effects on the stability of the system. Semi-active control systems, which can vary the stiffness and damping in real time, demonstrate better control effects than passive systems and consume less power than the active systems. Additionally, semi-active control devices can behave as passive devices in the event of a power loss, and are therefore more reliable [5–7]. Utilizing the performance benefits of semi-active control devices, the concept of a semi-active tuned mass damper (STMD) has been introduced in recent years. Hidaka et al. [8] conducted an experimental study of an STMD system coupled with a three-story building model under support ground motion. Pinkaew and Fujino [9] studied the control effectiveness of an STMD with variable damping under harmonic excitation. Varadarajan and Nagarajaiah [10] developed an STMD using a variable stiffness device and they have shown its effectiveness analytically and experimentally by using a small-scale three story structural model. Koo

* Corresponding author. Tel.: +82 53 810 2429; fax: +82 53 810 4625.
E-mail addresses: hskim72@sunmoon.ac.kr (H.-S. Kim), kangj@ynu.ac.kr (J.-W. Kang).

0141-0296/$ - see front matter © 2012 Elsevier Ltd. All rights reserved.
http://dx.doi.org/10.1016/j.engstruct.2012.03.038

et al. [11] presented an experimental robustness analysis of a semi-active tuned vibration absorber (TVA) subject to structural mass off-tuning using a magnetorheological (MR) damper.

One of the most promising semi-active devices is the MR damper. MR dampers are controllable fluid devices that employ MR fluids of which the rheological properties may be rapidly varied by an applied magnetic field. They can provide large force capacity, high stability, robustness and reliability. Furthermore, they are relatively inexpensive to manufacture and maintain and are insensitive to temperature so that they may be used for indoor and outdoor applications. Because of their mechanical simplicity, high dynamic range and low power requirements, they are considered to be good candidates for reducing structural vibrations and they have been studied by a number of researchers for seismic protection of civil structures [12–17].

Based on these background studies, a semi-active MR TMD (MR-STMD) is expected to be a promising control device for mitigating the wind-induced responses of a tall building structure. One of the challenges in the application of the MR-STMD is developing an appropriate control algorithm to determine the command voltage of the MR damper. Many control algorithms have been proposed to control the behavior of MR dampers or other semi-active devices. Skyhook and groundhook control policies [18,19], decentralized bang-bang control [20], the methods based on the Lyapunov theory [21], clipped-optimal control [22] and modulated homogeneous friction control [23] are some of the control algorithms used for semi-active control devices. Each of these control strategies has its own merits and limitations depending on the application and desired response. Also, note that the above-mentioned studies mainly focus on enhancement of the control performance of the semi-active control devices. However, in addition to the control performance, a constraint on the maximum allowable stroke of the MR-STMD is important for practical application and it must be considered in the design of the MR-STMD. To limit the stroke of the MR-STMD, overdamping or an additional damper may therefore be necessary, which results in a lower control efficiency of the MR-STMD, and thus in a larger response of the building structure. Since reduction of dynamic responses of the building structure is in conflict with reduction of the control device stroke, a multi-objective optimization approach is required in the design of semi-active control algorithms for the MR-STMD.

In this study, a multi-objective optimal semi-active control strategy for the response reduction of wind-excited tall buildings has been proposed. Because of the inherent robustness and ability to handle nonlinear systems and uncertainties, a fuzzy logic controller (FLC) is used in this study to operate an MR damper which is a key component of the MR-STMD. Although FLC has been used to control a number of structural systems, the selection of acceptable fuzzy membership functions has been subjective and time-consuming. To overcome this difficulty, a genetic algorithm (GA) is applied to the optimal design of FLC in this study. As mentioned above, because FLC should appropriately reduce both building structure and MR-STMD responses that are in conflict, a multi-objective optimization approach is introduced to the design of FLC. A multi-objective genetic algorithm is used to tune the membership functions and generate the rule base of a Mamdani type fuzzy controller [24].

In order to evaluate the performance of the proposed control method, a 76-story benchmark building subjected to wind excitation [25] is used as a numerical example structure. This benchmark building model is widely used by many researchers to verify control performance of control algorithms and devices [26,27]. The MR-STMD is installed on the top floor of the example building such as the passive TMD and ATMD presented in the benchmark problem. The benchmark problem specification [25] requires that the participants achieve the target control performance and to satisfy the control device capacity constraints simultaneously. To meet this requirement, a multi-objective optimization scheme that uses the Non-dominated Sorting Genetic Algorithm version II (NSGA-II) [28] is used in this study to determine the rule set of the FLC. NSGA-II has been demonstrated to be one of the most efficient algorithms for multi-objective optimization problems on a number of benchmarks. For comparative purposes, a sky–ground hook control algorithm is employed in numerical simulation for control of the MR-STMD. The effectiveness of the MR-STMD controlled by the control algorithm developed in this study is compared with that of the passive TMD and ATMD proposed in the benchmark problem [25]. Also, an investigation is carried out to determine whether the proposed control system can satisfy the design requirements and constraints provided in the benchmark problem.

2. Example building structure and performance evaluation criteria

2.1. 76-Story benchmark building model

The structural model used in this study is the benchmark building of a 76-story, 306-m tall concrete office tower proposed for the city of Melbourne, Australia [25]. The building has a square cross section with chamfers at two corners as shown in Fig. 1. This is a reinforced concrete building consisting of a concrete core and concrete frame. The core was designed to resist the majority of wind loads whereas the frame was designed to primarily carry the gravitational loads and part of the wind loads. The building is slender with a height to width ratio of 7.3. Therefore, it is wind sensitive. The total mass of the building, including the heavy machinery in the plant rooms, is 153,000 tons.

The 76-story tall building is modeled as a vertical cantilever beam (Bernoulli–Euler beam). A finite element model is constructed by considering the portion of the building between two adjacent floors as a classical beam element of uniform thickness, leading to 76 translational and 76 rotational degrees of freedom. Then, all the 76 rotational degrees of freedom have been removed by the static condensation. This results in a 76 degrees of freedom (DOF), representing the displacement of each floor in the lateral direction. This model, having (76×76) mass, damping, and stiffness matrices, is referred to as the "76 DOF model". The building with an ATMD is referred to as the "77 DOF model". The numerical computation of the controlled response quantities, including peak response, RMS response, etc., may be time consuming and computationally expensive for the 76 DOF and 77 DOF models. Hence the so-called state order reduction method has been used to derive

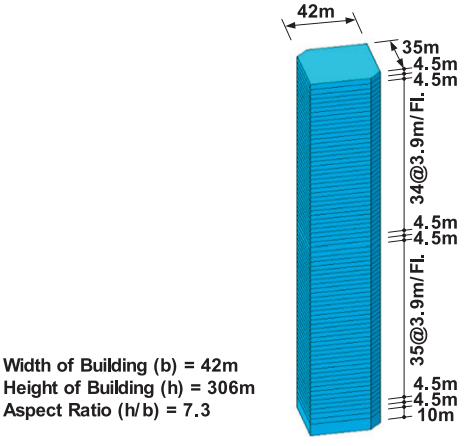

Fig. 1. 76-Story benchmark building model.

lower order models for the building with and without ATMD [25]. In this method, eigenvalues and eigenvectors of the selected modes of the full-order system are preserved in the reduced-order system. Based on this approach, the 77 DOF model (with ATMD) is reduced to a 24 DOF system such that the first 48 complex modes (eigenvalues and eigenvectors) of the 77 DOF system are retained. Similarly, the 76 DOF model (building without ATMD) is reduced to a 23 DOF system by retaining the first 46 complex modes of the original system. A more detailed explanation of the building model and numerical analysis method is provided in the benchmark problem [25].

Since the coupled lateral–torsional motion is neglected in the benchmark problem and across-wind and along-wind loads are uncorrelated, building response quantities due to across-winds and along-winds can be computed independently. Based on wind tunnel data, building response quantities due to across-wind loads are much higher than those due to along-wind loads. Consequently, only the design of a controller using across-wind loading is considered in the benchmark problem. Therefore, a two-dimensional analytical model is used and the rotations of the floors about the vertical axis are not considered in the numerical simulation. The resulting system of equations involving mass, stiffness, and damping matrices of the structure is solved by the Newmark-Beta integration scheme using a linear acceleration method [29]. The first five natural frequencies of the structure are 0.16, 0.765, 1.992, 3.790 and 6.395 Hz, respectively. Damping ratios for the first five modes are assumed to be 1% of the critical for the proportional damping matrix. The benchmark building is a long period structure having the first natural period of 6.25 s. Since the motion of a long period structure is generally governed by the first modal response, the frequencies of the TMD, ATMD and MR-STMD have been tuned to the first modal frequency of the structure. The sample ATMD proposed in the benchmark problem has the same mass and location as the TMD. A control algorithm for the sample ATMD was designed based on the linear quadratic Gaussian (LQG) theory. Wind forces acting on the benchmark building were obtained by wind tunnel tests. A rigid model of the 76-story benchmark building was constructed and tested in the boundary layer wind tunnel facility at the Department of Civil Engineering at the University of Sydney, Australia [30]. For the performance evaluation of control systems, only the first 15 min of across-wind data are used. Based on the design code for office buildings in Australia, the maximum allowable floor acceleration is 15 cm/s^2, with an RMS acceleration of 5 cm/s^2 [31]. This is a serviceability requirement. The design constraints specified for the benchmark problem are the RMS control force $\sigma_u \leqslant 100$ kN, the RMS actuator stroke $\sigma_{xm} \leqslant 30$ cm, the maximum control force $\max|u(t)| \leqslant 300$ kN and the maximum stroke $\max|x_m(t)| \leqslant 95$ cm. More detailed information on the evaluation criteria and benchmark problem can be found in the benchmark definition paper by Yang et al. [25].

2.2. Performance evaluation criteria for MR-STMD

To evaluate the control system performance the following twelve indices introduced in the benchmark problem must be considered [25]. From the response time histories, the peak response quantities can be obtained and the temporal RMS values can be computed. The main objective of installing control systems on the tall building is to reduce the absolute acceleration to alleviate the occupant's discomfort; however, no consideration is given to the frequency dependence of human perception to acceleration. The first evaluation criterion for the controllers is their ability to reduce the maximum floor RMS acceleration. A non-dimensional version of this performance criterion is given by

$$J_1 = \max(\sigma_{\ddot{x}1}, \sigma_{\ddot{x}30}, \sigma_{\ddot{x}50}, \sigma_{\ddot{x}55}, \sigma_{\ddot{x}60}, \sigma_{\ddot{x}65}, \sigma_{\ddot{x}70}, \sigma_{\ddot{x}75})/\sigma_{\ddot{x}75o} \quad (1)$$

where $\sigma_{\ddot{x}i}$ = RMS acceleration of the ith floor and $\sigma_{\ddot{x}75o} = 9.142$ cm/s^2 = RMS acceleration of the 75th floor without control. In the performance criterion J_1, accelerations only up to the 75th floor are considered because the 76th floor is the top of the building and it is not used by the occupants.

The second criterion is the average performance of acceleration for selected floors above the 49th floor, i.e.

$$J_2 = \frac{1}{6}\sum_i(\sigma_{\ddot{x}i}/\sigma_{\ddot{x}io}); \quad \text{for } i = 50, 55, 60, 65, 70 \text{ and } 75 \quad (2)$$

in which $\sigma_{\ddot{x}io}$ = RMS acceleration of the ith floor without control. The third and fourth evaluation criteria are the ability of the controller to reduce the top floor displacements. The normalized versions are given as follows:

$$J_3 = \sigma_{x76}/\sigma_{x76o} \quad (3)$$

$$J_4 = \frac{1}{7}\sum_i(\sigma_{xi}/\sigma_{xio}); \quad \text{for } i = 50, 55, 60, 65, 70, 75 \text{ and } 76 \quad (4)$$

where σ_{xi} and σ_{xio} = RMS displacements of the ith floor with and without control, respectively, and $\sigma_{x76o} = 10.137$ cm is the RMS displacement of the 76th floor of the uncontrolled building. In addition to the constraints of a proposed control design, its control effort requirements should be evaluated in terms of the following non-dimensionalized actuator stroke and average power:

$$J_5 = \sigma_{xm}/\sigma_{x76o} \quad (5)$$

$$J_6 = \sigma_p = \left\{\frac{1}{T}\int_0^T [\dot{x}_m(t)u(t)]^2 dt\right\}^{1/2} \quad (6)$$

in which σ_{xm} = RMS actuator stroke, $\dot{x}_m(t)$ = actuator velocity, T = total time of integration, and σ_p denotes RMS control power.

In addition to the RMS performance, the performance in terms of the peak response quantities is also important. This set of non-dimensional performance criteria is given in the following:

$$J_7 = \max(\ddot{x}_{p1}, \ddot{x}_{p30}, \ddot{x}_{p50}, \ddot{x}_{p55}, \ddot{x}_{p60}, \ddot{x}_{p65}, \ddot{x}_{p70}, \ddot{x}_{p75})/\ddot{x}_{p75o} \quad (7)$$

$$J_8 = \frac{1}{6}\sum_i(\ddot{x}_{pi}/\ddot{x}_{pio}); \quad \text{for } i = 50, 55, 60, 65, 70 \text{ and } 75 \quad (8)$$

$$J_9 = x_{p76}/x_{p76o} \quad (9)$$

$$J_{10} = \frac{1}{7}\sum_i(x_{pi}/x_{pio}); \quad \text{for } i = 50, 55, 60, 65, 70, 75 \text{ and } 76 \quad (10)$$

where x_{pi} and x_{pio} = peak displacements of the ith floor with and without control, respectively, and $\ddot{x}_{pi}$ and $\ddot{x}_{pio}$ = peak accelerations of the ith floor with and without control, respectively, for instance, x_{p76o} = 32.30 cm and $\ddot{x}_{p75o} = 30.33$ cm/s^2. In addition, the proposed control designs should be evaluated for the following control capacity criteria:

$$J_{11} = x_{pm}/x_{p76o} \quad (11)$$

$$J_{12} = P_{\max} = \max_t|\dot{x}_m(t)u(t)| \quad (12)$$

where x_{pm} = peak stroke of actuator, $u(t)$ = control force, and $P_{\max}$ = peak control power. From the performance criteria defined above, it is observed that as the performance of the controller improves, the values of the performance indices decrease.

3. Dynamic model of MR-STMD

As described previously, an MR damper is employed to compose a semi-active TMD system instead of a passive damping device as

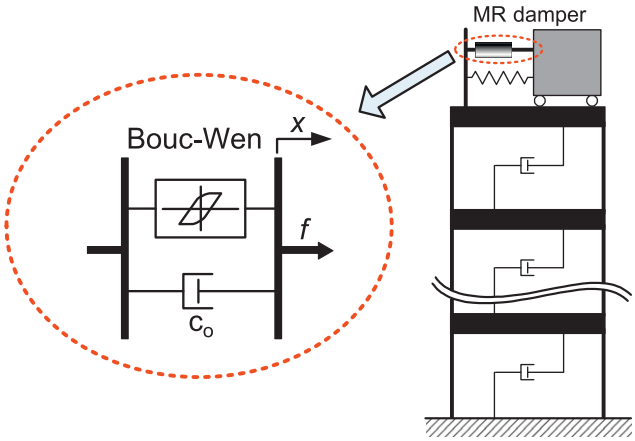

Fig. 2. Configuration of semi-active tuned mass damper.

shown in Fig. 2. In this study, the Bouc-Wen model [32] is used to describe how the damping force is related to the velocity and applied command voltage. The mechanical model for the MR damper based on the Bouc-Wen hysteresis model is shown in Fig. 2. The force f generated by the MR damper is calculated by

$$f = c_0\dot{x} + \alpha z \tag{13}$$

$$\dot{z} = -\gamma|\dot{x}||z|^{n-1} - \beta\dot{x}|z|^n + A\dot{x} \tag{14}$$

where $\dot{x}$ and c_0 are the velocity and viscous damping of the MR damper, and z is the evolutionary variable. As shown in Eq. (14), the hysteretic behavior of the MR damper is expressed by a first-order differential equation. The variables γ, β, n, and A are adjustable shape parameters of the hysteresis loops for the yielding element in the MR damper [32]. These variables can control the linearity in the unloading and the smoothness of the transition from the pre-yield to the post-yield region. The model parameters of the MR damper governing equation, α and c_0 are functions of the applied voltage v as follows

$$\alpha = \alpha_a + \alpha_b u \tag{15}$$

$$c_0 = c_{0a} + c_{0b} u \tag{16}$$

$$\dot{u} = -\eta(u - v) \tag{17}$$

where u and v are the input and output voltages of the first-order filter and η is the time constant of the first-order filter. The variables α_a, α_b, c_{0a} and c_{0b} are parameters that account for the dependence of the MR damper force on voltages applied to the current driver and the resulting magnetic current [33]. Note that unlike the active devices, semi-active devices can produce dissipative forces only in the same direction as the velocity of the damper. In addition, there is an upper and lower limit on the force produced by the MR damper which depends on the damper velocity at any considered time.

The MR damper parameters used in this study are selected so that the device has a capacity of approximately 100 kN, as follows; α_a = 21744 N/cm, α_b = 99232 N/(cm V), c_{0a} = 0.88 N s/cm, c_{0b} = 8.8 N s/(cm V), n = 1, A = 1.2, γ = 3 cm^{-1}, β = 3 cm^{-1}, and η = 50 s^{-1}. These parameters are based on an identified model of an MR damper tested at Washington State University [34] and scaled down to have a maximum generated force of about 100 kN depending on the relative velocity across the MR damper with a saturation voltage of 5 V. Accordingly, the voltage applied to the MR damper is within the range 0–5 V. The model of the MR damper presented in Eqs. (13)–(17) was encoded in SIMULINK [35]. Typical force velocity/displacement hysteresis loops for this device model are generated using the coded model and are shown in Fig. 3. According to what said above, in the event of a power loss, MR-STMD will act as a passive TMD.

For a comparative study, the inertial mass of the MR-STMD used in this study is identical to that of the passive TMD and ATMD presented in the benchmark problem, i.e. 500 tons. This is about 45% of the top floor mass, which is 0.327% of the total mass of the building. The single MR-TMD is installed on the top floor of the 76-story benchmark building. The undamped natural frequency of the MR-STMD is 0.16 Hz, which is the first mode natural frequency of the example building.

4. Control algorithms

To date, numerous control algorithms have been adopted for semi-active control systems. These include skyhook damper control algorithm proposed for a vehicle suspension system [18]. This was followed by a decentralized bang-bang controller [20], direct Lyapunov based control algorithms [21], a modified homogeneous friction algorithm [23] and widely used clipped optimal strategy [22]. These algorithms provide either zero or the maximum voltage value (without any intermediate levels of voltage supply) to the MR damper based on feedback from the structure. Thus these methods provide sub-optimal control force to the system. Moreover, swift changes in command voltage lead to a sudden rise in the external control force which increases the structural responses and may introduce local damages in the structure. Therefore, there is a need for control algorithms that can change the command voltage sent to the MR damper gradually and smoothly. This gradual change in MR damper supply voltage will enable a designer to cover all voltage values between zero and the maximum voltage value.

This paper provides an optimal fuzzy logic controller to calculate the command voltage. Some characteristics of FLC appealing to control engineers are their effectiveness and ease in handling structural nonlinearities, uncertainties and heuristic knowledge. Added to the niceties present in a fuzzy system, a fuzzy control applied to structural system can handle the hysteretic behavior of the structure under earthquake [36]. Moreover, it provides an added robustness to the closed loop system when combined with MR dampers. Another advantage of the FLC used in conjunction with MR damper is that unlike in clipped optimal and Lyapunov control techniques, the change in command voltage sent to the MR damper is gradual and therefore it covers all voltage values in the range of zero and maximum MR damper voltages. This particular advantage not only permits the designer to use variable voltage value but also provides an inherent stability to the closed loop system [36]. To show this characteristics of FLC, the command voltage time history generated by FLC is presented later in this paper.

The performance of FLC depends on various design parameters related to selection of membership functions and definition of rule base. It is especially important for FLC to have an effective and reliable rule base to perform at the desired level. Although FLC results in the creation of simple control algorithms, the tuning of the fuzzy controller is a more difficult and sophisticated procedure than that employed in conventional control algorithms (e.g., clipped optimal algorithm, Lyapunov methods, etc.). That is, the design of fuzzy control rules to drive the MR damper voltage is challenging since it requires a good understanding of the dynamic response of the structure with the MR-STMD which has a highly nonlinear behavior. To overcome this difficulty, a multi-objective genetic algorithm (MOGA) is applied to the optimal design of FLC in this study. The development process of the MOGA-optimized FLC will be described in Section 5. The limitation to be considered in GA optimization is that it needs intensive computational efforts for objective

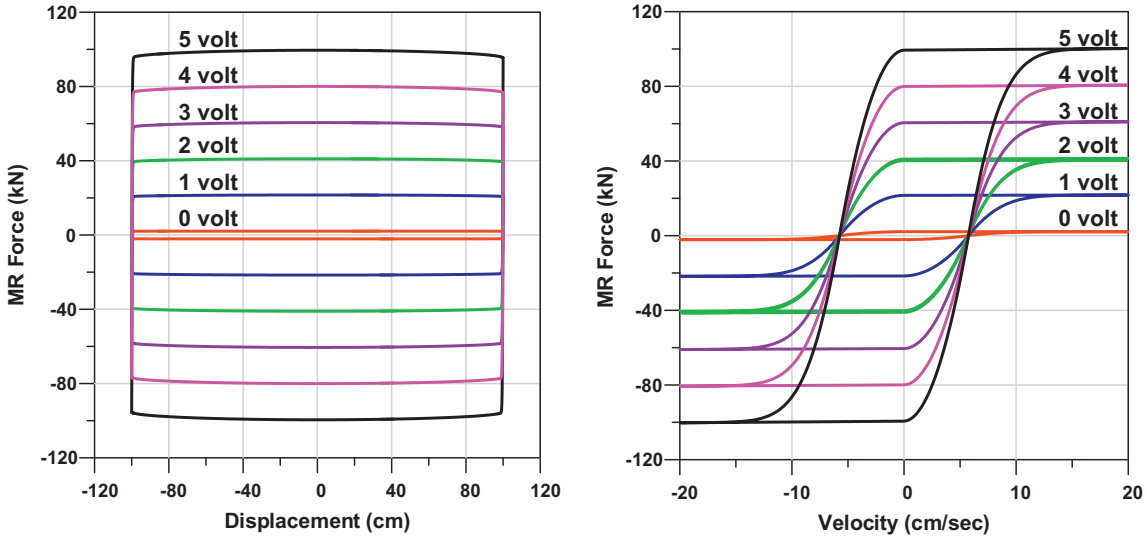

(a) force-displacement hysteresis loop (b) force-velocity hysteresis loop

Fig. 3. Hysteresis loops of the MR damper.

function evaluations in comparison with conventional optimization methods. This limitation is discussed in detail in Section 6.

4.1. Fuzzy logic control algorithm

As explained previously, an FLC is employed in this study to operate an MR damper. An FLC maps an input space to an output space and the primary mechanism for doing this is a list of if–then statements called fuzzy rules. In this study, the MR-STMD stroke and the 75th floor acceleration are selected for two input variables of the FLC and the output variable is the command voltage sent to the MR damper. The if-part of the rule is called the antecedent, while the then-part of the rule is called the consequent. As presented in Fig. 4, interpreting an if–then rule involves distinct parts: first evaluating the antecedent (which involves fuzzifying the input and applying any necessary fuzzy operators) and second applying that result to the consequent (known as implication). All fuzzy statements are resolved in the antecedent to a degree of membership between 0 and 1. To describe this process more specifically, an example fuzzy if–then rule with specific inputs is used as shown in Fig. 4. An example fuzzy rule is "if the STMD stroke is MF1_R1 and the 75th floor acceleration is MF2_R1 then the command voltage is MF3_R1". Here, MF1_R1, MF2_R1 and MF3_R1 stand for membership functions of the fuzzy rule 1 and the parameters of these membership functions are determined by NSGA-II in the next section. Let's assume that input 1 (the MR-STMD stroke) is 27 cm and input 2 (the 75th floor acceleration) is 9.2 cm/s^2. In this case, the input 1 and the input 2 correspond to 0.8 for MF1_R1 and 0.5 for MF2_R1, respectively as shown in Fig. 4. In this manner, each input is fuzzified over all the qualifying membership functions required by the rules. After the input values are entered and fuzzified, the fuzzy operator is applied to the antecedent and two fuzzified results, i.e. 0.8 and 0.5, are resolved to a single number of 0.5. In this study, the 'minimum' function is used

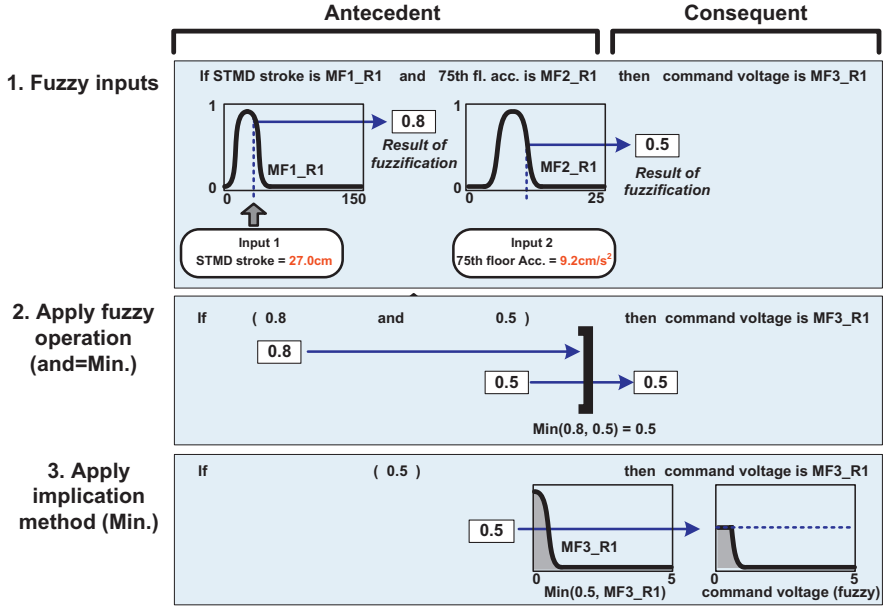

Fig. 4. Interpretation of if–then rules.

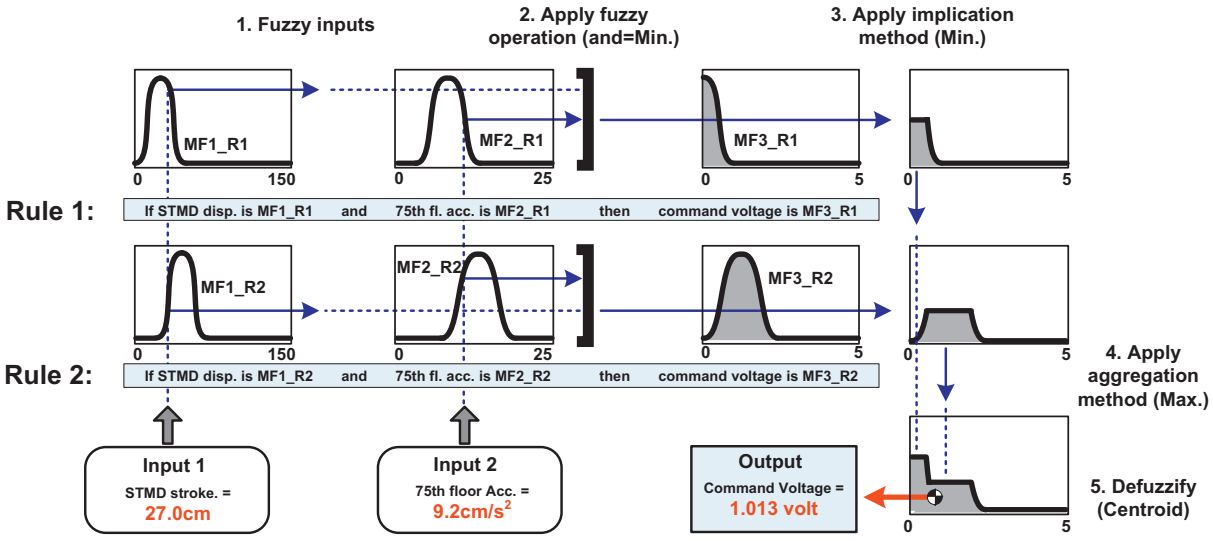

Fig. 5. Five steps of fuzzy logic controller.

for the 'and' fuzzy operator. If the antecedent is assigned a value less than 1, then the output fuzzy set is truncated according to the implication method using the 'minimum' function as shown in Fig. 4. This truncated fuzzy set will later be defuzzified, assigning one value to the output command voltage. The concept of defuzzification is described below.

In this study, 20 fuzzy rules are used for the fuzzy logic control algorithm. Generally, an input may be involved in more than one rule and this is a characteristics of fuzzy reasoning. In this case, all if–then rules are evaluated in parallel, and the order of the rules is unimportant. After all fuzzy rules are evaluated, the results of the rules are combined and deffuzified to a single number output. In order to explain this process more clearly, Fig. 5 is employed. It shows the process of formulating the mapping from a given input to an output using fuzzy logic including if–then rule interpretation through five steps. Step 1: Fuzzy inputs. Step 2: Apply fuzzy operator. Step 3: Apply implication method. Step 4: Aggregate all outputs. Step 5: Defuzzify [37]. Based on Fig. 5, the value of input 1 (27 cm) is partially included in MF1_R1 and it is also included in MF1_R2 in the rule 2. The 75th floor acceleration of 9.2 cm/s^2 for input 2 is included in both of MF2_R1 and MF2_R2. The rule 1 and rule 2 out of 20 fuzzy rules are involved in this example. After interpreting two if–then fuzzy rules, two truncated output fuzzy sets are obtained as shown in Fig. 5. The truncated output fuzzy sets for each rule are then aggregated into a single output fuzzy set by the 'maximum' function. Finally the resulting set is defuzzified to a single number. For defuzzification, the centroid calculation which is the most popular defuzzification method is used in this study. Consequently, the output command voltage is 1.013 in this example. If input 1 is changed from 27 cm to 28 cm, the output command voltage is promptly calculated by simple computation. Through this process, an FLC allows fine resolution in output command voltage.

4.2. Comparative control algorithm

In order to verify the control performance of the MOGA-optimized FLC, a comparative control algorithm is introduced in this study. A comparative control algorithm is developed by using skyhook and groundhook control algorithms which are typical semi-active control algorithms. For civil structure applications, a skyhook controller can effectively reduce the vibration of the auxiliary mass, i.e. the MR-STMD. On the other hand, a groundhook controller shows good control performance for the reduction of structure responses [38]. The idealized configurations of both the skyhook and groundhook controllers are shown in Fig. 6. These ideal skyhook and groundhook configurations cannot be realized in practice because the damper cannot be fixed to the sky or a non-moving inertia frame. Therefore, the goal of skyhook or groundhook semi-active control policies is to emulate the ideal structural configuration of a passive damper "hooked" between the structure and the "sky" or the "ground", respectively, by using the real configuration of the MR-STMD as shown in Fig. 2. Among various versions of groundhook control algorithms, the displacement-based on–off groundhook controller is employed in this study because it shows the best performance for the benchmark problem among the four control policies investigated by Koo et al. [19].

Referring to Fig. 6, the relative velocity is defined by subtracting the velocity of the MR-STMD from that of the structure, i.e. $v_1 - v_2$. The displacement-based skyhook control policy is defined by using the relative velocity and the displacement of the MR-STMD (x_2). In the case of the on–off skyhook control algorithm, the command voltage is switched between a minimum and a maximum level. The switching is performed based on the following conditions:

$$V = \begin{cases} V_{\max} & \text{if } x_2(v_1 - v_2) \leqslant 0 \\ V_{\min} & \text{if } x_2(v_1 - v_2) > 0 \end{cases} \tag{18}$$

where V is the command voltage, $V_{\max}$ is the maximum voltage, namely 5 V, and $V_{\min}$ is the minimum voltage, 0 V.

The displacement-based on–off skyhook control policy can be evolved to the groundhook control policy by changing x_2 to x_1. The groundhook control algorithm used in this study is given by:

$$V = \begin{cases} V_{\max} & \text{if } x_1(v_1 - v_2) \geqslant 0 \\ V_{\min} & \text{if } x_1(v_1 - v_2) < 0 \end{cases} \tag{19}$$

As observed in Eqs. (18) and (19), the command voltage based on skyhook or groundhook control is determined by a very simple computation. Because of this simplicity, they have been favorably used for real-time control and successfully applied to civil structure control with good performance.

To combine two control commands provided by groundhook and skyhook controllers, an appropriate combination method is required. There are several methods that can be used to combine multiple control signals to make a single control command. One

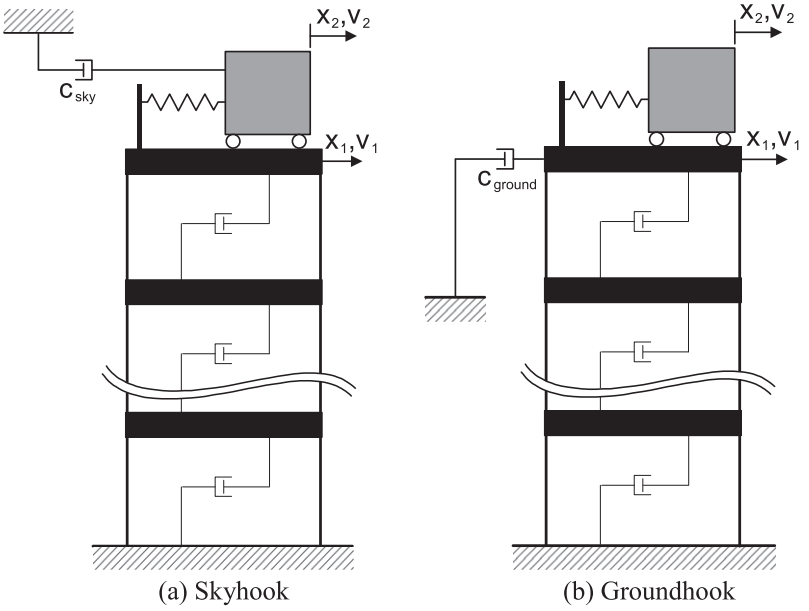

Fig. 6. Idealized semi-active control configurations (for comparative control strategies).

of these methods, a weighted sum approach, is widely used because of its simplicity and intuitive understanding. Using the conventional weighted sum approach, two control commands from groundhook and skyhook controllers can be easily combined as follows:

$$V = wV_{sky} + (1 - w)V_{ground} \tag{20}$$

where V is the combined command voltage, V_{sky} is the command voltage generated by the skyhook controller, V_{ground} is the command voltage provided by the groundhook controller, and w is a weighting factor. In this combination method, the participation of each controller can be conveniently adjusted by changing the weighting factor. Eleven numerical simulation runs, where w varied from 0 to 1 in steps of 0.1, have been conducted to determine an appropriate weighting factor that can satisfy the design requirement of the benchmark problem. As observed in Eq. (20), if w is smaller than 0.5, the participation of the skyhook controller decreases in comparison with the groundhook controller. In this case, the structure displacement decreases and the MR-STMD displacement increases. On the other hand, as the weighting factor (w) increases, the participation of the skyhook controller increases, but the effect of the groundhook controller is reduced. Therefore, the combined control command in this case shows good control performance for the reduction of MR-STMD movement rather than for structure responses. In this study, the value of 0.5 is selected for the weighting factor to make a sky–ground hook control algorithm that can appropriately reduce both building structure and MR-STMD responses that are in conflict.

5. Development of multi-objective optimal fuzzy control algorithms

5.1. Optimization with multi-objective genetic algorithm

As described previously, the design purposes of FLC for the MR-STMD applied to the 76-story benchmark building can be separated into two aspects; that is, one is the reduction of the dynamic responses of the building structure and the other is the reduction of the MR-STMD movement. Thus, the design procedure of the FLC can be thought of as a multi-objective process that finds optimal

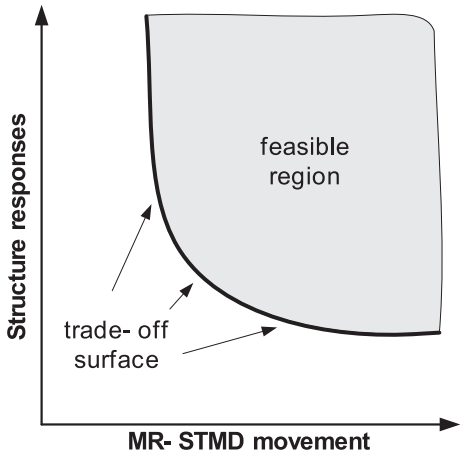

Fig. 7. Trade-off between MR-STMD movement and structure responses.

solutions that show superior control with respect to several performance indices. Multi-objective optimization is the search for acceptable solutions to problems that incorporate multiple performance criteria. It should be noted that a common difficulty with multi-objective optimization is the conflict of objectives; that is, none of the feasible solutions allow simultaneous optimal solutions for all objectives. When a trade-off exists between the objectives, an improvement in one objective cannot be achieved without detriment to another. It is very rare for a multi-objective optimization problem to admit a single optimal solution; rather, a family of equally valid solutions (Pareto optimal solutions) exists.

In the case of structural control of a tall building with an MR-STMD subjected to wind excitation, a trade-off exists between the MR-STMD movement and the dynamic responses of the building structure (i.e., a reduction of the building structure responses cannot be achieved without an increment of the MR-STMD movement, whereas the MR-STMD movement can be reduced with an increment of the building structure responses) as shown in Fig. 7. For example, if the damping force of an MR damper is increased in order to reduce MR-STMD movement, the dynamic responses

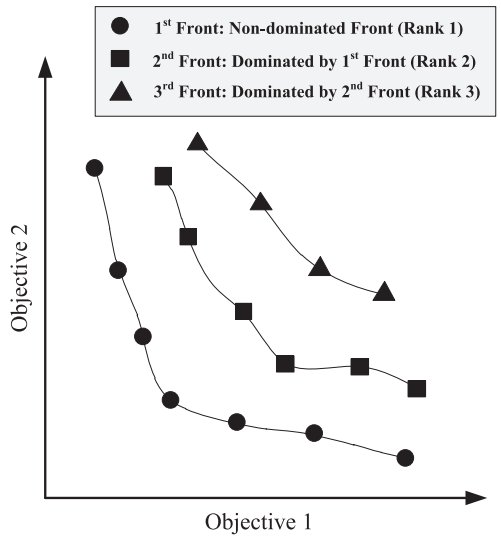

Fig. 8. Non-dominated sorting concept.

of the building structure manifest a concomitant increase. Conversely, structure responses can be reduced by decreasing the MR damper force, but can lead to increased MR-STMD movement. Therefore, it is impossible for minimum displacement of the MR-STMD and minimum acceleration of the building structure to occur simultaneously. In this study, the reduction of peak and RMS responses of the MR-STMD movement and the 75th floor acceleration are selected as four objectives in a multi-objective optimization process because the top of the building (76th floor) is not used by the occupants.

In solving multi-objective structural engineering problems, engineers may be interested in a set of Pareto optimal solutions that provide alternative structural designs for a controller, instead of a single solution. Since a genetic algorithm (GA) works with a population of solutions, it seems natural to use a GA in multi-objective optimization problems in order to capture a number of optimal solutions simultaneously. Since Schaffer [39] first applied a GA to multi-objective optimization problems, a number of multi-objective evolutionary algorithms have been suggested [26,39–41]. Among many available GA-based multi-objective optimization strategies, the fast elitist Non-dominated Sorting Genetic Algorithm version II (NSGA-II) is employed in this study [28]. The computational time in NSGA-II is significantly reduced in comparison with existing multi-objective GAs and the crowding operator is introduced to maintain diversity without specifying any additional parameters.

5.2. Optimization of FLC using NSGA-II

Deb et al. have proposed an elitist, fast, and parameter-free multi-objective GA denoted as NSGA-II. Essentially, NSGA-II has a unique characteristic compared to conventional multi-objective GAs in a number of ways. Firstly, NSGA-II uses an elite preserving mechanism, thereby assuring preservation of previously found good solutions. Secondly, NSGA-II uses a fast non-dominated sorting procedure. Thirdly, NSGA-II does not require a tunable parameter, thereby making the algorithm independent of the user. The essential difference between a multi-objective GA and a single objective GA is the method by which fitness is assigned to potential solutions. Each solution has a vector describing its performance across the set of multiple criteria. This vector must be transformed into a single scalar fitness value for the purpose of the GA selection mechanism. The transformation is achieved by ranking the population of solutions relative to each other, and then assigning a fitness value that is based on rank. Individual solutions are compared in terms of Pareto dominance. In this procedure, the population of each generation is searched for non-dominated solutions. If solution 's1' is better than solution 's2' for both objectives then solution 's1' is said to dominate over solution 's2' or in other words one can say that solution 's2' is dominated by solution 's1.' If a solution is dominated by one or more other solutions, the solution can be discarded, or else it can be retained in the population. After a comparison of all the solutions in this way, all of the retained solutions are non-dominated solutions and form a set of Pareto-optimal solutions. This set of solutions is assigned a rank of 1 and they are then temporarily removed from the original population. Similarly, non-dominated solutions are then identified in the remaining population, and these solutions are assigned a rank of 2 and are removed from contention. The process continues until all individuals have been ranked as shown in Fig. 8. In effect, this process creates a series of non-dominated fronts. Deb et al. adopted this approach for NSGA-II. Multi-objective ranking, which impacts primarily on fitness assignment, is the key difference between a multi-objective GA (MOGA) and a standard GA. To get an estimate of the density of solutions surrounding a particular solution in the population, the average distance of the two solutions on either side of the selected

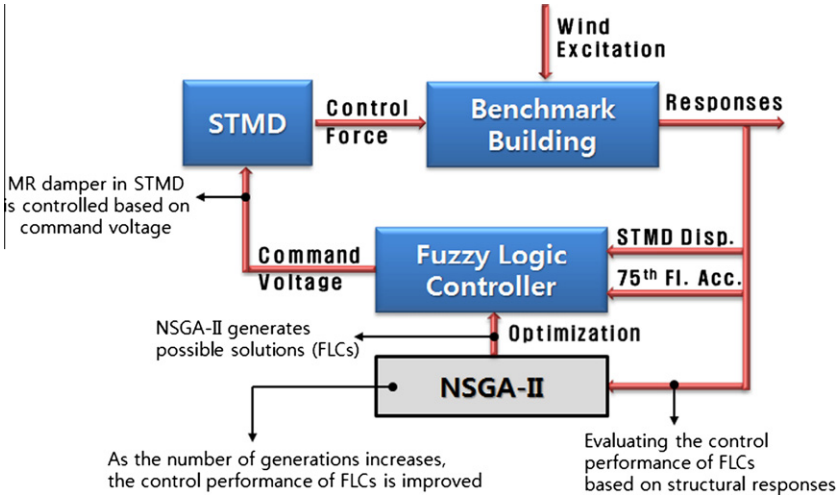

Fig. 9. Flow of optimization of fuzzy logic controller using NSGA-II.

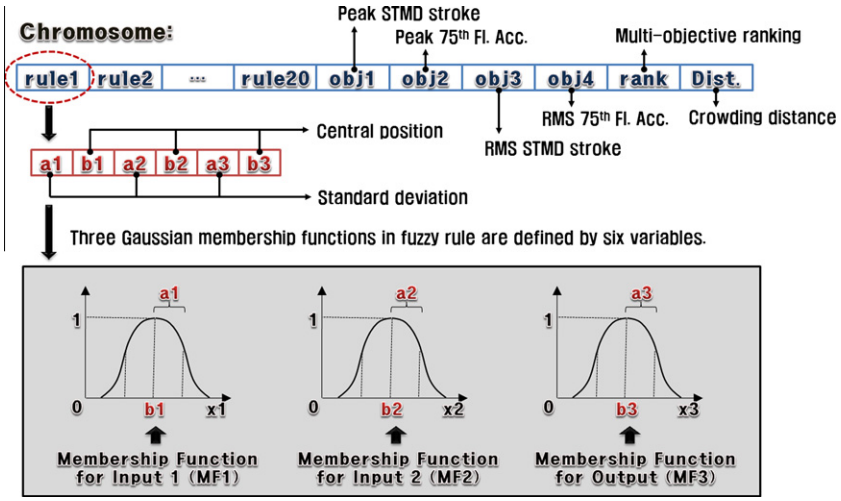

Fig. 10. Encoding structure of a chromosome in NSGA-II.

solution along each of the objectives is computed. This quantity serves as an estimate of the size of the largest cuboid enclosing the solution without including any other solution in the population. Deb et al. term this metric the 'crowding distance.' The crowded comparison operator guides the selection process at various stages of the algorithm towards a uniformly spread out Pareto optimal front. Every individual in the population has two attributes introduced previously, that is, a non-domination rank and a local crowding distance. In NSGA-II optimization, between two solutions with different non-domination ranks the solution with the lower rank is preferred. Otherwise, if both the solutions belong to the same front then the solution is preferred which is located in a region with a lesser number of solutions. A solution point with a larger cuboid enclosing it is given priority. Note that diversity among non-dominated solutions is introduced by using this crowding comparison procedure which is used in the tournament selection operator. Since solutions compete with their crowding distance, no extra niching parameter is required.

The optimization procedure for an FLC using NSGA-II is presented in Fig. 9. After evaluating the control performance of an FLC based on structural responses, NSGA-II optimizes the FLC toward improvement of control performance. Encoding is the genetic representation of an FLC solution. All of the information represented by the FLC parameters is encoded in a structure called a chromosome or string. For purposes of control of the 76-story benchmark building, two inputs, i.e. the MR-STMD displacement and the 75th floor acceleration of the building structure, and one output, the command voltage to the MR damper, are selected as shown in Fig. 9. Gaussian membership functions are used for all input and output variables of the FLC because they can approximate almost all other types of membership functions by changing the parameters shown in Eq. (21).

$$\mu = \exp\left(-\frac{(x-b)^2}{2a^2}\right) \tag{21}$$

The shape of a Gaussian membership function can be defined by two parameters: b and a. Here, b is the central position, and a is the width (standard deviation) as shown in Fig. 10. Using these two parameters, various types of knowledge can be expressed. These two parameters are encoded into the gene with a real-valued representation. For each chromosome there are two inputs, $x1$ and $x2$, and one output, $x3$, in each rule. A rule has the parameters of Eq. (21), i.e. the central positions $b1$ and $b2$ and the width $a1$ and $a2$, for inputs $x1$ and $x2$, respectively. For output x3, the central position $b3$ and the width $a3$ are encoded. As shown in Fig. 10, 20 fuzzy rules are used in this study. Fitness values for each objective ($obj1$, $obj2$, $obj3$, $obj4$) are also encoded in the latter part of the chromosome

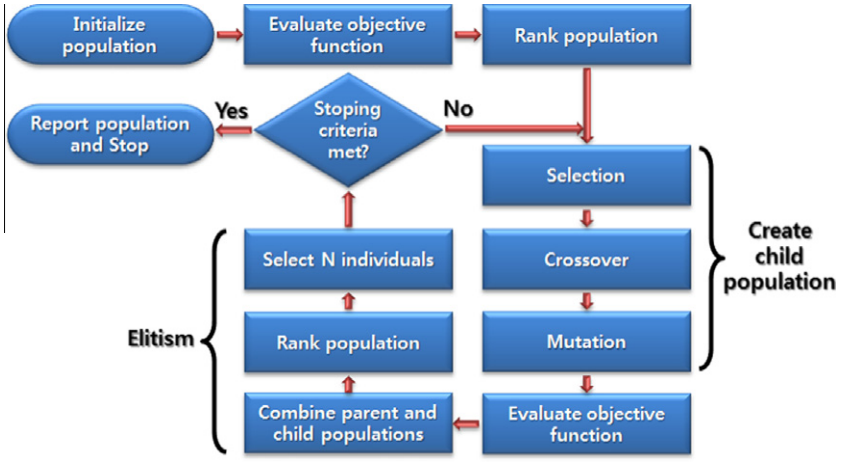

Fig. 11. Flowchart of NSGA-II.

and they are used to evaluate each chromosome by NSGA-II. After evaluation, multi-objective ranking (*rank*) and crowding distance (*Dist.*) are saved in the chromosome.

An optimization procedure through NSGA-II is shown in Fig. 11. Initially, the population of size *N* is composed of completely randomized values that reside within a user-defined range. After evaluating the control performance of all individuals in the population, a non-domination rank and a local crowding distance of each individual are calculated. After that, the fundamental GA operators such as selection, crossover and mutation are used to create the child population. Crossover occurs when parent chromosomes exchange equal amounts of information to produce a child. In this study all individuals in the parent population are subjected to a crossover to produce the child population. The crossover process is a tournament style procedure where two randomly selected chromosomes exchange a portion of their chromosomes in a single point exchange. Occasionally data are changed at random during the crossover to keep the generation cycle from becoming static; this operation is termed a mutation. After the child population is created and the control performances of each individual in the child population are evaluated, the parent and child populations are combined. This combined population is sorted according to non-domination concept described previously. The new parent population is formed by adding solutions to the next generation starting from the first front until N individuals are found. This process continues until stopping criteria is met.

6. Numerical studies

A numerical model of the 76-story benchmark building structure with the MR-STMD is implemented in SIMULINK. SIMULINK is a graphical extension to MATLAB for modeling and simulation of systems. It is integrated with MATLAB and data can be easily transferred between the programs [35]. A SIMULINK model with a control device is provided in the benchmark problem to easily simulate the features and limitations of the structural control problem and to compute both the RMS and peak response quantities as well as the performance indices. This SIMULINK model has been modified in this study to include the MR-STMD and FLC as shown in Fig. 12. Using this numerical model, time history analyses of 900 s with a time step of 0.001 s are performed in order to investigate the control performance of the MR-STMD controlled by the NAGA-II optimized FLC. As described above, the NSGA-II based optimization is performed with the population size of 100 individuals. An upper limit on the number of generations is specified to be 1000. As the number of generations increases, the control performance of the elite (i.e. non-dominated) individuals is improved. Evolution processes of fitness values for peak and RMS responses are presented in Figs. 13 and 14, respectively. Since evolution process of single fitness value is meaningless in multi-objective optimization problem, fitness values for MR-STMD displacement and structure acceleration that are in conflict are presented together. As can be seen in figures, the Pareto optimal fronts improve rapidly in the early generations, when the individuals are farther from the optimum. The Pareto optimal fronts improve more slowly in later generations, whose populations are closer to the optimal front.

After the multi-objective optimization process for FLC using NSGA-II, the obtained Pareto optimal fronts (a set of Pareto optimal solutions) are presented with the comparative control algorithm in Figs. 15 and 16. In these figures, the NSGA-II optimized FLCs are presented in "NSGA-II" and the comparative control algorithm introduced in Section 4.2 is presented in "Sky–Ground Hook". As can be seen in Figs. 15 and 16, the NSGA-II optimized FLCs can provide better control performance than the comparative sky–ground hook control algorithm in both peak and RMS responses. Especially in peak response control, the NSGA-II optimized FLCs can significantly reduce the MR-STMD displacement while providing improved performance in reducing structure acceleration compared to the comparative sky–ground hook control algorithm.

In general, the MR-STMD displacement responses are in competition with the structure acceleration responses. Therefore, the objectives for reduction of peak and RMS 75th floor accelerations of the benchmark building can be improved at the cost of the degraded objectives for the reduction of peak and RMS strokes of the MR-STMD. Therefore, the engineer needs to choose a proper FLC that can satisfy the desired performance requirements and constraints on the control device. Consequently, one controller has been selected among the Pareto optimal FLCs and it is

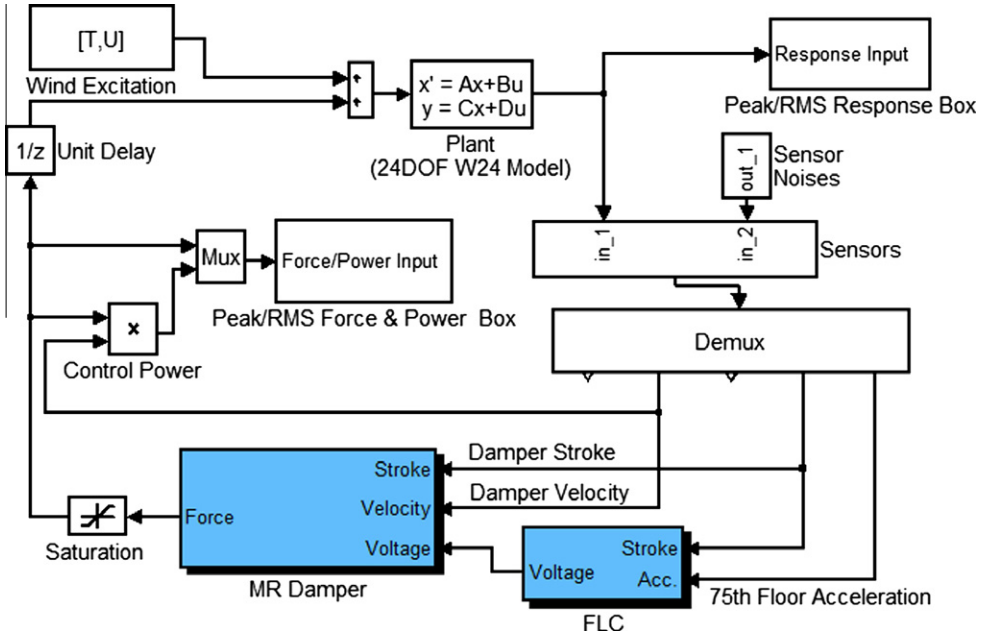

Fig. 12. SIMULINK model of the building with fuzzy logic controller.

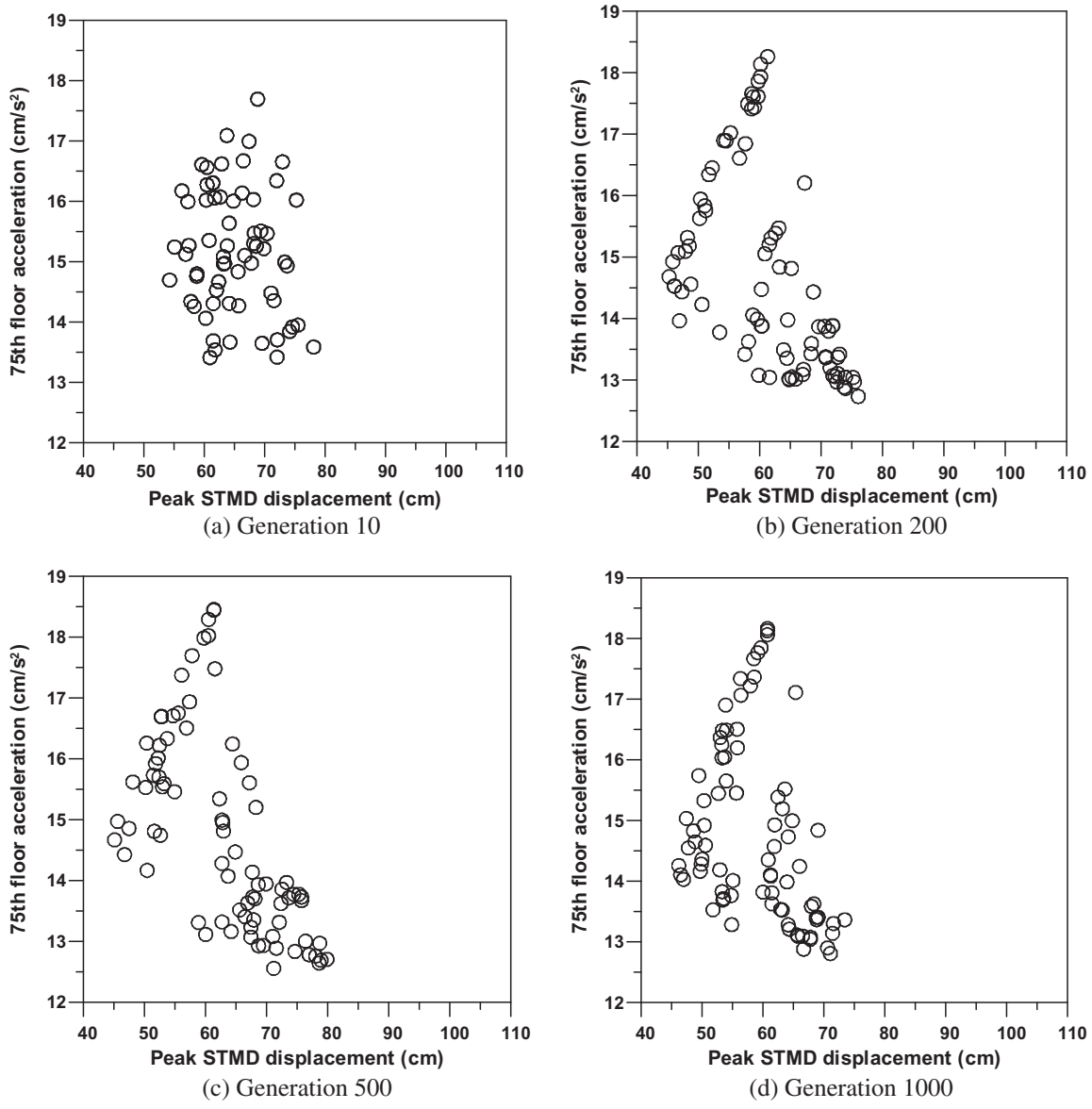

Fig. 13. Evolution process of the fitness for two objectives of peak responses.

presented as a solid circle in Figs. 15 and 16. The parameter values of the selected FLC are provided in Table 1. Twenty fuzzy rules can be directly generated by means of 'if–then' statement shown in Fig. 10. If only peak responses are considered in selecting an appropriate FLC, there are many FLCs which provide better control performance than the selected FLC as shown in Fig. 15. However, because the reduction of RMS responses of the structure, as well as peak responses, is important for occupants' comport, an FLC presented as a solid circle is selected in this study. In other words, the FLCs with lower acceleration values and similar peak STMD displacement compared to the selected FLC in Fig. 15 provide worse control performance in RMS response reduction compared to the selected FLC in Fig. 16.

When the MR-STMD displacement and the 75th floor acceleration of the building subjected to wind excitation are sent to the selected FLC, the command voltage to control the MR damper is determined promptly. The time history of the command voltage provided by the selected FLC is presented in Fig. 17. It can be seen that the command voltage varies between '0 V' and '5 V' during real-time control. In general, the FLC provides high voltage for the MR damper in order to reduce the MR-STMD movement if the dynamic response of the MR-STMD is considerable. On the other hand, when the 75th floor acceleration is significant, the command voltage sent to the MR damper is decreased to increase the MR-STMD movement resulting in the effective control of the dynamic responses of the structure. The mean value of the command voltage time history generated by the FLC is 1.61 V, which is significantly less than the maximum voltage of 5 V. This means that the selected FLC emphasizes the reduction of the structure response rather than the MR-STMD movement. This is because the FLC that can effectively reduce the 75th floor acceleration rather than the MR-STMD displacement is selected among the Pareto optimal FLCs as shown in Figs. 15 and 16. If the engineer wants an FLC that can effectively reduce the MR-STMD displacement, a different FLC having the desired characteristics can be simply selected from the Pareto optimal FLCs.

The control performance of the groundhook, skyhook, sky–ground hook ($w = 0.5$) and NSGA-II optimized FLC for the wind-excited benchmark building with the MR-STMD are compared to those of the passive TMD and ATMD presented in the benchmark

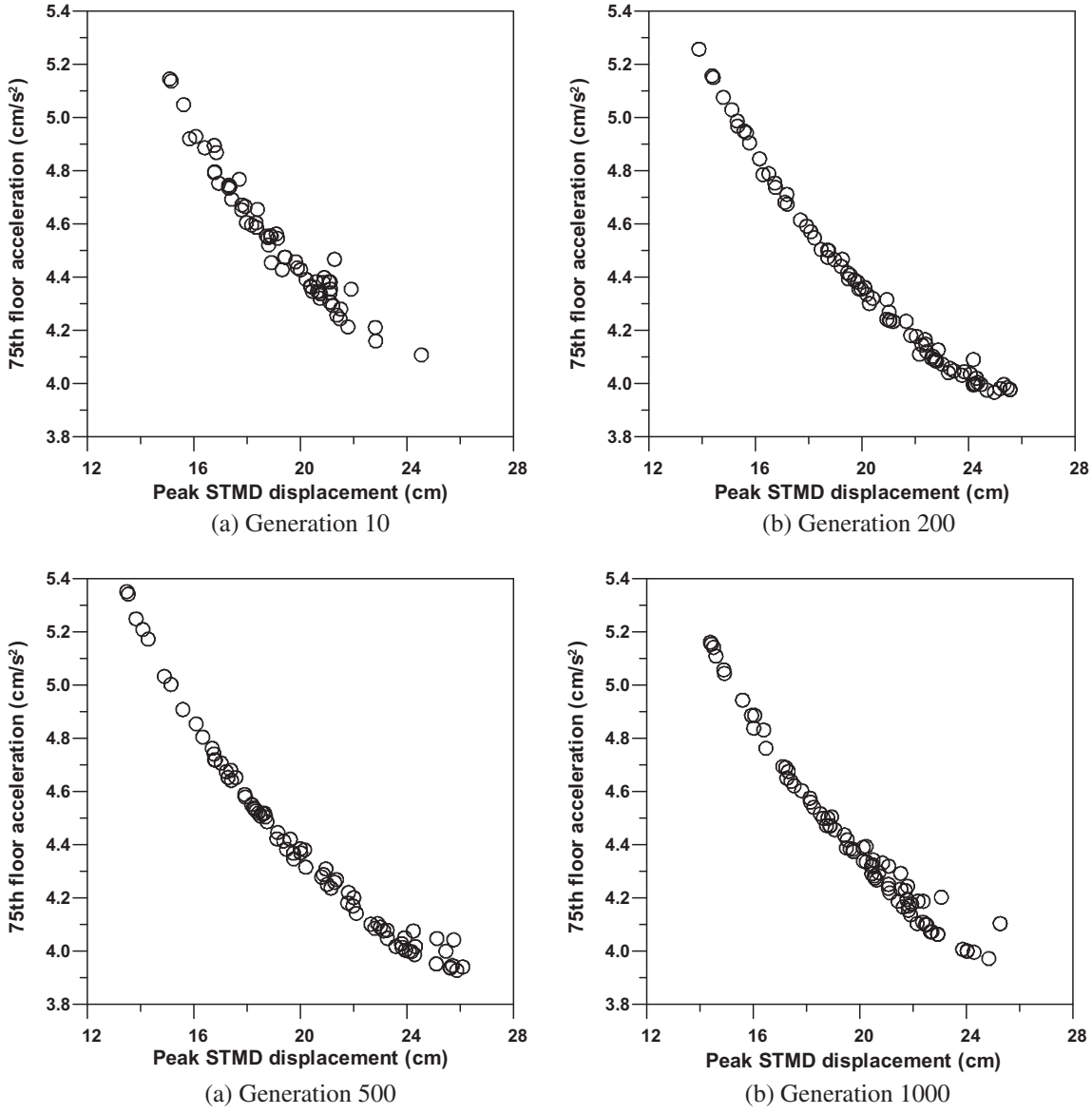

Fig. 14. Evolution process of the fitness for two objectives of RMS responses.

problem [25]. To this end, the peak and RMS response quantities for the selected floors (levels 1, 30, 50, 55, 60, 65, 70, 75, and 76) are summarized in Tables 2 and 3. For the passive TMD, the peak and RMS acceleration response quantities on the 75th floor (19.79 cm/s^2 and 5.38 cm/s^2) are larger than the allowable peak and RMS floor acceleration, i.e. 15 cm/s^2 and 5 cm/s^2. Thus, the passive TMD does not satisfy the design requirement of the benchmark building. When the ATMD is used, the response of the mass damper increases compared to the TMD. However, it satisfies the design requirement when excluding the 76th floor, which has no occupants. In the case of the MR-STMD, groundhook, skyhook, sky–ground hook ($w = 0.5$) and NSGA-II optimized FLC are employed as stated above. When a groundhook controller is used, the peak and RMS accelerations of the 75th floor are 13.36 cm/s^2 and 3.91 cm/s^2, respectively, and they are less than the maximum allowable floor acceleration of 15 cm/s^2 and the RMS value of 5 cm/s^2, respectively. However, the peak and RMS displacements of the MR-STMD are 106.32 cm and 30.74 cm, respectively, as shown in Tables 2 and 3. They exceed the control constraints given by 95 cm and 30 cm, respectively. On the other hand, a skyhook controller can easily satisfy the control constraints of the MR-STMD displacement by providing the peak value of 66.89 cm and the RMS value of 16.99 cm. However, the peak acceleration of the 75th floor is 16.60 cm/s^2, which is greater than the maximum allowable floor acceleration. Based on numerical simulation, it is found that neither of the two controllers can satisfy the design requirement of the benchmark building on their own. When the sky–ground hook controller with the weighting factor of 0.5 is employed, both the MR-STMD movement and the 75th floor acceleration are appropriately controlled. That is, the sky–ground hook controller reduces structural responses better than the skyhook controller but the MR-STMD movement is increased compared to the skyhook controller. On the other hand, the sky–ground hook controller can control the MR-STMD movement better than the groundhook controller though structural responses of the sky–ground hook controller are bigger than those of the groundhook controller. Consequently, the sky–ground hook controller can satisfy the design requirement when excluding the 76th floor. When the NSGA-II optimized FLC is used for control of the MR-STMD, the peak and RMS responses of the structure are similar to those

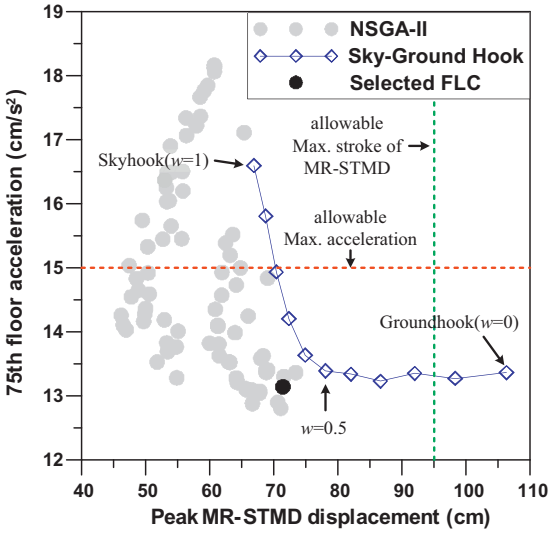

Fig. 15. Optimization results (peak response).

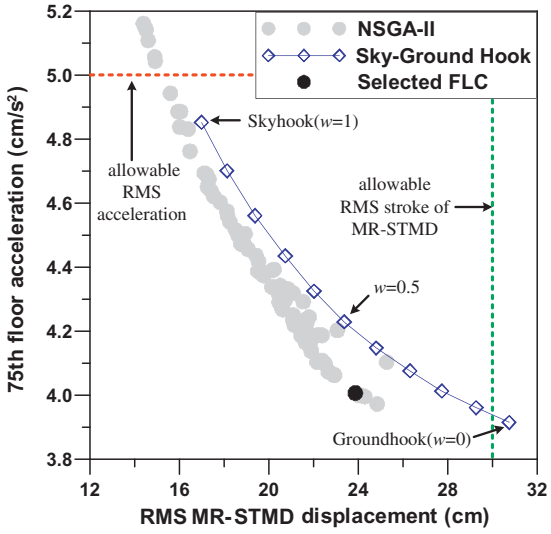

Fig. 16. Optimization results (RMS response).

Table 1
Parameter values of optimized fuzzy logic controller.

	*a*1	*b*1	*a*2	*b*2	*a*3	*b*3
Rule1	17.41	23.90	1.12	6.32	0.20	−0.02
Rule2	4.81	−53.67	2.27	−2.75	0.08	−0.92
Rule3	12.70	−74.89	0.45	−6.96	0.05	−0.74
Rule4	0.01	−87.26	1.17	2.50	0.11	−0.29
Rule5	11.84	−39.11	2.21	−7.55	0.06	−0.19
Rule6	19.22	−42.10	1.76	5.57	0.05	−0.58
Rule7	20.84	−59.57	0.77	6.73	0.01	0.85
Rule8	10.98	−99.52	2.04	2.32	0.02	−1.18
Rule9	5.41	66.26	0.68	−5.48	0.03	−1.18
Rule10	17.69	−39.56	1.90	6.76	0.01	−0.10
Rule11	11.30	69.92	2.07	0.11	0.10	−1.10
Rule12	22.37	9.23	0.14	−7.55	0.03	0.13
Rule13	4.47	56.02	1.90	−0.71	0.05	−0.77
Rule14	10.71	−5.12	1.57	−3.84	0.17	0.23
Rule15	4.22	−53.71	0.90	5.59	0.01	0.33
Rule16	6.52	20.63	1.62	7.82	0.15	0.18
Rule17	7.27	−6.60	2.01	−6.76	0.03	−1.14
Rule18	4.00	75.27	1.01	−9.33	0.18	−0.31
Rule19	16.95	8.59	0.48	−2.30	0.05	0.57
Rule20	18.49	−77.40	2.34	−2.25	0.14	−0.94

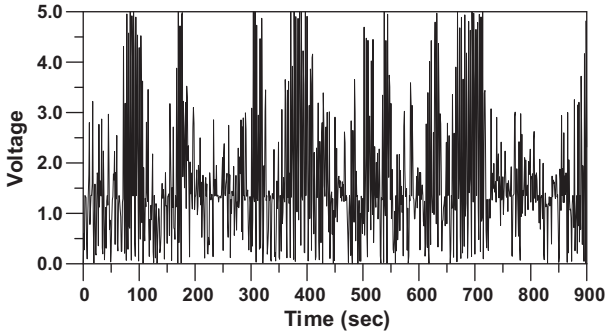

Fig. 17. Time history of command voltage.

of the groundhook controller and the MR-STMD movement is significantly reduced in comparison with the groundhook controller. The peak and RMS structural responses of the NSGA-II optimized FLC are smaller than those of the sky–ground hook controller. All the dynamic responses of the benchmark building having MR-STMD controlled by NSGA-II optimized FLC are significantly reduced compared to the passive TMD. Moreover, the peak displacement response quantities of all the floors are less than those of the ATMD. The peak and RMS stroke of the MR-STMD are 71.46 cm and 23.87 cm, respectively, which are less than the prescribed limit. Numerical results show that the MR-STMD controlled by NSGA-II optimized FLC satisfies the design requirement including the 76th floor.

Performance evaluation criteria of MR-STMD controlled by groundhook, skyhook, sky–ground hook and NSGA-II optimized FLC are shown with those of the passive TMD and ATMD in Table 4. A comparison between groundhook and skyhook controllers shows that the groundhook controller provides considerably better control performance for all the structure responses than the skyhook controller. On the other hand, the performance criteria associated with the MR-STMD response (J_5 and J_{11}) of the groundhook controller are inferior to those of the skyhook controller. As expected, the control performance of the sky–ground hook controller lies between those of the skyhook and groundhook controllers. The control performance of the NSGA-II optimized FLC is comparable to that of the groundhook controller, but with a significant reduction in the MR-STMD response. Table 4 shows that the control performance of the MR-STMD controlled by the NSGA-II optimized FLC is superior to that of the passive TMD. In comparison with the ATMD, the MR-STMD provides a good performance for reduction in displacement response (J_3, J_4, J_9 and J_{10}) while the ATMD shows better control performance criteria associated with acceleration responses (J_1, J_2, J_7 and J_8). It should be noted that the average and peak control power (J_6 and J_{12}) of the MR-STMD are significantly smaller than those of the ATMD, while it provides a similar control performance.

The acceleration and displacement time histories of the 75th floor are shown in Figs. 18 and 19 for the cases of the TMD and MR-STMD, including the uncontrolled case. The structure responses with the TMD and MR-STMD are significantly less than those of the uncontrolled case. As observed in Figs. 18 and 19, the structure response with the MR-STMD is less than that with the TMD.

Specifically, the difference between the control performances of the TMD and MR-STMD is significant around 700 s, where the responses of the benchmark building are most excessive. Accordingly, the MR-STMD appears to be effective for controlling excessive vibrations that can cause severe damage to the structure. The MR-STMD stroke time history is also presented in Fig. 20. As can be seen in this figure, a greater movement of the MR-STMD

Table 2
Comparison of peak structural response quantities.

Floor No.	MR-STMD								TMD		ATMD	
	Groundhook		Skyhook		Sky–ground hook ($w = 0.5$)		NSGA-II optimized FLC					
	Disp.	Acc.	Disp.	Acc.	Disp.	Acc.	Disp.	Acc.	Disp.	Acc.	Disp.	Acc.
1	0.04	0.22	0.04	0.21	0.04	0.21	0.04	0.21	0.04	0.21	0.04	0.23
30	4.93	3.74	5.47	4.15	5.19	3.84	4.89	3.75	5.60	4.68	5.14	3.37
50	11.69	7.18	13.04	8.26	12.35	7.65	11.60	6.93	13.34	9.28	12.22	6.73
55	13.60	8.23	15.18	9.21	14.38	8.43	13.49	8.23	15.54	10.74	14.22	8.05
60	15.56	9.37	17.38	10.76	16.45	9.47	15.44	9.04	17.80	12.70	16.27	8.93
65	17.56	10.26	19.63	12.33	18.57	11.05	17.42	10.03	20.10	14.72	18.36	10.05
70	19.58	11.67	21.90	13.99	20.72	12.44	19.42	11.31	22.43	16.77	20.48	10.67
75	21.67	13.36	24.25	16.60	22.93	14.80	21.49	13.14	24.84	19.79	22.67	11.56
76	22.14	14.53	24.77	17.34	23.43	15.46	21.95	14.38	25.38	20.52	23.15	15.89
MR-STMD	106.32	109.06	66.89	72.40	69.53	73.25	71.46	78.42	42.60	46.18	74.27	72.64

Table 3
Comparison of RMS structural response quantities.

Floor No.	MR-STMD								TMD		ATMD	
	Groundhook		Skyhook		Sky–ground hook ($w = 0.5$)		NSGA-II optimized FLC					
	Disp.	Acc.	Disp.	Acc.	Disp.	Acc.	Disp.	Acc.	Disp.	Acc.	Disp.	Acc.
1	0.01	0.06	0.01	0.06	0.01	0.06	0.01	0.06	0.01	0.06	0.01	0.06
30	1.24	0.95	1.40	1.14	1.33	1.06	1.26	0.97	1.48	1.23	1.26	0.89
50	2.99	2.02	3.37	2.54	3.22	2.34	3.03	2.08	3.57	2.79	3.04	2.03
55	3.49	2.34	3.94	2.95	3.76	2.72	3.54	2.41	4.17	3.26	3.55	2.41
60	4.01	2.66	4.53	3.36	4.32	3.08	4.06	2.73	4.79	3.72	4.08	2.81
65	4.54	3.05	5.13	3.84	4.89	3.53	4.60	3.13	5.43	4.25	4.62	3.16
70	5.08	3.42	5.75	4.33	5.48	3.98	5.15	3.52	6.08	4.76	5.17	3.38
75	5.64	3.91	6.38	4.85	6.08	4.48	5.71	4.01	6.75	5.38	5.74	3.34
76	5.77	3.98	6.52	4.98	6.22	4.58	5.84	4.08	6.90	5.48	5.86	4.70
MR-STMD	30.74	30.55	16.99	18.03	19.58	20.31	23.87	23.96	12.76	13.86	23.03	22.4

Table 4
Comparison of performance criteria (note: lower value indicates higher performance).

Index	Description		MR-STMD				TMD	ATMD
			Ground hook	Skyhook	Sky–ground hook ($w = 0.5$)	NSGA-II optimized FLC		
J_1	RMS response	Max. acc.	0.428	0.531	0.490	0.438	0.589	0.369
J_2		Avg. acc.	0.420	0.528	0.485	0.431	0.583	0.417
J_3		Max. disp.	0.569	0.643	0.613	0.576	0.681	0.578
J_4		Avg. disp.	0.571	0.645	0.615	0.578	0.682	0.580
J_5		Actuator stroke	3.032	1.676	1.931	2.354	1.258	2.271
J_6		Control power	3.237	1.808	2.082	2.532	1.358	11.988
J_7	Peak response	Max. acc.	0.441	0.547	0.488	0.433	0.652	0.381
J_8		Avg. acc.	0.461	0.541	0.487	0.450	0.637	0.432
J_9		Max. disp.	0.685	0.767	0.725	0.679	0.786	0.717
J_{10}		Avg. disp.	0.694	0.775	0.734	0.688	0.794	0.725
J_{11}		Actuator stroke	3.292	2.071	2.153	2.211	1.319	2.299
J_{12}		Control power	3.494	2.167	2.246	2.341	1.384	71.869

is required to reduce the excessive response of the building. Furthermore, it can be recognized that the peak MR-STMD stroke is less than the maximum allowable STMD stroke (i.e. 95 cm).

In addition to the control performance, robustness is one of the most important features of control devices. The benchmark problem suggested that the robustness of the proposed controller should be discussed because the variation of the structure's frequency may cause significant performance deterioration. To investigate the robustness of the proposed MR-STMD, the performance criteria of the passive TMD and MR-STMD are compared for stiffness uncertainties of ±15% as shown in Table 5. Among the twelve criteria, only eight criteria (J_1–J_4 and J_7–J_{10}) are used because the other criteria represent the performance of the mass damper. Numerical results show that the robustness of the MR-STMD is superior to that of the passive TMD, although the control effects of the MR-STMD are deteriorated with stiffness variation. In the case of the passive TMD under a stiffness uncertainty of −15%, J_{10} is slightly larger than '1'. In this case, the peak displacements of the building with TMD are less than those without TMD in the upper stories, but the peak displacements controlled by TMD are larger than the uncontrolled responses in the lower stories. Performance index of J_{10} is the average value of the peak displacements for selected floors as described previously. Consequently, it is calculated to be slightly larger than 1 though the peak displacement of top floor is reduced by passive TMD.

The main disadvantage of GA optimization is that it needs intensive objective function evaluations and thus it is sort of slow compared to conventional optimization methods. Numerical

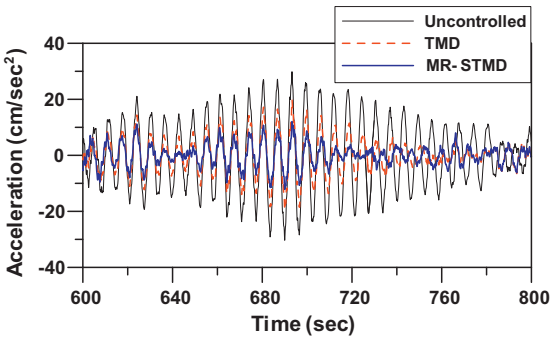

Fig. 18. Acceleration time history of the 75th floor.

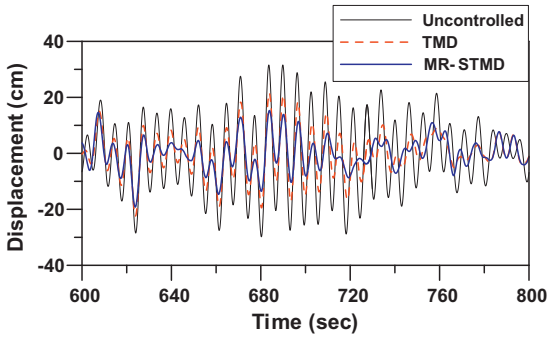

Fig. 19. Displacement time history of the 75th floor.

simulation for 900 s with a time step of 0.001 s under the environment of SIMULINK requires really high computational time. Although a state order reduction method was used to derive the 24 DOF model of a 76-story building structure for efficient numerical computation, computational time is considerable for searching the optimal solutions of fuzzy controller. In this study, numerical simulation time for one generation takes approximately 4 h by using a computer with Core i7 3.4 GHz processor, 8.0 GB RAM, and Matlab R2009b 64-bit. In order to reduce the computational efforts for objective function evaluation, a time step of 0.001 and/or a simulation duration of 900 s can be modified. Much research has been conducted on the improvement of the efficiency of GA optimization [42,43]. If this advanced GA technique is applied to the optimization of fuzzy controller, the optimization time is expected to be considerably reduced.

7. Conclusions

This study investigates the control performance of a semi-active TMD with an MR damper (MR-STMD) for a 76-story tall building subjected to wind excitation. In order to effectively control the MR-STMD, a fuzzy logic controller is employed in this study and it is optimized by a multi-objective genetic algorithm (NSGA-II). After an optimization run using NSGA-II, an engineer can select an appropriate FLC that satisfies the desired performance requirements from among a number of Pareto optimal solutions. Since skyhook and groundhook control algorithms can effectively reduce the dynamic responses of the MR-STMD and the building structure, respectively, they are used as comparative controllers. The sample passive TMD and ATMD proposed in the benchmark problem are also used as references for comparative studies.

Based on numerical simulations, it can be seen that the NSGA-II optimized FLC can effectively reduce both responses of the MR-STMD and building structure compared to the sky–ground hook control algorithm. The MR-STMD controlled by the proposed FLC

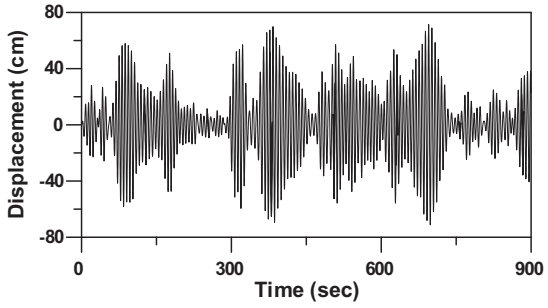

Fig. 20. MR-STMD stroke time history.

Table 5
Robustness of TMD and MR-STMD.

RMS responses					Peak responses				
Index	$\Delta K = -15\%$		$\Delta K = +15\%$		Index	$\Delta K = -15\%$		$\Delta K = +15\%$	
	TMD	MR-STMD	TMD	MR-STMD		TMD	MR-STMD	TMD	MR-STMD
J_1	0.594	0.544	0.494	0.468	J_7	0.695	0.663	0.556	0.544
J_2	0.586	0.535	0.488	0.464	J_8	0.697	0.622	0.557	0.524
J_3	0.809	0.775	0.526	0.517	J_9	0.999	0.868	0.633	0.639
J_4	0.810	0.776	0.527	0.516	J_{10}	1.008	0.874	0.637	0.648

shows significantly better control performance than the passive TMD. Generally, the control performance of the MR-STMD is comparable to that of the ATMD, whereas the control power of the MR-STMD is substantially lower than that of the ATMD. For the reduction of the acceleration responses, the ATMD shows a better control performance than the MR-STMD. However, the MR-STMD can effectively reduce the displacement responses compared to the ATMD. For changes in stiffness of the structure, the MR-STMD controlled by the proposed controller is less sensitive than the passive TMD. However, even if an MR-STMD shows better control performance than the passive TMD, an engineer should carefully consider the introduction of an MR-STMD by weighing the performance improvement against the additional cost associated with managing a semi-active control system. Consequently, the design requirements of the benchmark problem have been successfully achieved by the proposed control method while satisfying the control device capacity constraints. Since the MR-STMD with an MR damper having a reasonable capacity (100 kN) is successfully used to control the full-scale 76-story building, the MR-STMD is expected to be a practical means for mitigating the wind-induced responses of a tall building. In research on this benchmark problem for response control of wind-excited tall buildings including this study, the same wind loads obtained from wind tunnel are used for both development and evaluation of controllers because only one set of across-wind data are provided in the benchmark problem. Accordingly, in order to increase confidence in the applicability of the control method proposed for this benchmark problem, other wind loads obtained from wind tunnel will be required to be used for performance evaluation.

Acknowledgment

This research was supported by the Yeungnam University research Grants in 2010.

References

[1] Den Hartog JP. Mechanical vibrations. New York: McGraw-Hill; 1956.
[2] Warburton GB. Optimum absorber parameters for various combinations of response and excitation parameters. Earthq Eng Struct Dynam 1982;10:381–401.

[3] Chang JCH, Soong TT. Structural control using active tuned mass damper. J Eng Mech 1980;106:1091–8.
[4] Ankireddi S, Yang HTY. Simple ATMD control methodology for tall buildings subject to wind loads. J Struct Eng 1996;122:83–91.
[5] Gaul L, Hurlebaus S, Wirnitzer J, Albrecht H. Enhanced damping of lightweight structures by semi-active joints. Acta Mech 2008;195:249–61.
[6] Yi F, Dyke S, Caicedo J, Carlson JD. Experimental verification of multi input seismic control strategies for smart dampers. J Eng Mech 2001;127(11):1152–64.
[7] Casciati F, Magonette G, Marazzi F. Technology of semiactive devices and applications in vibration mitigation. Chichester: Wiley & Sons; 2006.
[8] Hidaka S, Ahn YK, Morishita S. Adaptive vibration control by a variable-damping dynamic absorber using ER fluid. J Vib Acoust 1999;121:373–8.
[9] Pinkaew T, Fujino Y. Effectiveness of semi-active tuned mass dampers under harmonic excitation. Eng Struct 2001;23:850–6.
[10] Varadarajan N, Nagarajaiah S. Wind response control of building with variable stiffness tuned mass damper using empirical mode decomposition/hilbert transform. J Eng Mech 2004;130(4):451–8.
[11] Koo JH, Ahmadian M, Setareh M. Experimental robustness analysis of magneto-rheological tuned vibration absorbers subject to mass off-tuning. J Vib Acoust, Trans Am Soc Mech Eng 2006;128(1):126–31.
[12] Kim HS, Roschke PN, Lin PY, Loh CH. Neuro-fuzzy model of hybrid semi-active base isolation system with FPS bearings and an MR damper. Eng Struct 2006;28(7):947–58.
[13] Dyke SJ, Spencer BF, Sain MK, Carlson JD. Modeling and control of magnetorheological dampers for seismic response reduction. Smart Mater Struct 1996;5:565–75.
[14] Spencer BF, Dyke SJ, Sain MK, Carlson JD. Phenomenological model of a magnetor-heological damper. J Eng Mech 1997;123(3):230–8.
[15] Kim HS, Roschke PN. Design of fuzzy logic controller for smart base isolation system using genetic algorithm. Eng Struct 2006;28(1):84–96.
[16] Ok SY, Kim DS, Park KS, Koh HM. Semi-active fuzzy control of cable-stayed bridges using magneto-rheological dampers. Eng Struct 2007;29(5):776–88.
[17] Jung HJ, Choi KM, Spencer BF, Lee IW. Application of some semi-active control algorithms to a smart base-isolated building employing MR dampers. Struct Control Health Monit 2006;13:693–704.
[18] Narasimhan S, Nagarajaiah S, Johnson EA, Gavin HP. Smart base isolated benchmark building. Part I: problem definition. Struct Control Health Monit 2006;13:573–88.
[19] Koo JH, Setareh M, Murray TM. In search of suitable control methods for semi-active tuned vibration absorbers. J Vib Control 2004;10:163–74.
[20] Feng Q, Shinozuka M. Use of a variable damper for hybrid control of bridge response under earthquake. In: US national workshop on structural control research. University of Southern California, Los Angeles; 1990.
[21] Brogan WL. Modern control theory. Englewood Cliffs (NJ): Prentice-Hall; 1991.
[22] Dyke SJ, Spencer BF. Seismic response control using multiple MR dampers. In: 2nd International workshop on structural control. Hong Kong University of Science and Technology Research Center; 1996.
[23] Inaudi JA. Modulated homogeneous friction: a semi-active damping strategy. Earthq Eng Struct Dynam 1997;26(3):361–76.
[24] Mamdani EH, Assilian S. An experiment in linguistic synthesis with a fuzzy logic controller. Int J Man Mach Stud 1975;7(1):1–13.
[25] Yang JN, Agrawal AK, Samali B, Wu JC. Benchmark problem for response control of wind-excited tall buildings. J Eng Mech 2004;130(4):437–46.
[26] Min KW, Kim HS, Lee SH, Kim HJ, Ahn SK. Performance evaluation of tuned liquid column dampers for response control of a 76-story benchmark building. Eng Struct 2005;27:1101–12.
[27] Aldawod M, Samali B, Naghdy F, Kwok KCS. Active control of along wind response of tall building using a fuzzy controller. Eng Struct 2001;23:1512–22.
[28] Deb K, Pratap A, Agrawal S, Meyarivan T. A fast elitist non-dominated sorting genetic algorithm for multi-objective optimization: NSGA-II. IEEE Trans Evol Comput 2002;6(2):182–97.
[29] Ohtori Y, Christenson RE, Spencer Jr BF, Dyke SJ. Benchmark control problems for seismically excited nonlinear buildings. J Eng Mech 2004;130(4):366–85.
[30] Samali B, Kwok KCS, Wood GS, Yang JN. Wind tunnel tests for wind-excited benchmark building. J Eng Mech 2004;130(4):437–46.
[31] Australian/New Zealand Standard. Structural design actions: wind actions, AS1170·2. Standards Australia, Sydney; 2002.
[32] Sues RH, Mau ST, Wen YK. System identification of degrading hysteretic restoring forces. J Eng Mech 1988;114(5):833–46.
[33] Spencer BF, Dyke SJ, Sain MK, Carlson JD. Phenomenological model of a magnetorheological damper. J Eng Mech 1997;123(3):230–8.
[34] Yi F, Dyke SJ, Caicedo JM, Carlson JD. Experimental verification of multi-input seismic control strategies for smart dampers. J Eng Mech 2001;127(11):1152–64.
[35] The Math Works Inc. MATLAB R2009b, Natick, MA; 2009.
[36] Ali SF, Ramaswamy A. Optimal fuzzy logic control for MDOF structural systems using evolutionary algorithms. Eng Appl Artif Intell 2009;22:407–19.
[37] Yen J, Langari R. Fuzzy logic: intelligence, control, and information. New York: Prentice Hall, Inc.; 1999.
[38] Setareh M. Use of semi-active tuned mass dampers for vibration control of force-excited structures. Struct Eng Mech 2001;11(4):341–56.
[39] Schaffer JD. Multiple objective optimization with vector evaluated genetic algorithms. In: First international conference on genetic algorithms, Hillsdale, NJ; 1985. p. 93–100.
[40] Horn J, Nafpliotis N, Goldberg DE. A niched Pareto genetic algorithm for multiobjective optimization. In: First IEEE conference on evolutionary computation. Orlando (FL): IEEE Press; 1994. p. 82–7.
[41] Fonseca CM, Fleming PJ. Genetic algorithms for multiobjective optimization: formulation, discussion and generalization. In: Genetic algorithms: fifth international conference. Morgan Kaufmann, San Mateo, CA; 1993. p. 416–23.
[42] Lim D, Ong YS, Jin Y, Sendhoff B, Lee BS. Efficient hierarchical parallel genetic algorithms using grid computing. Future Gener Comput Syst 2007;23(4):658–70.
[43] Kwok YK, Ahmad I. Efficient scheduling of arbitrary task graphs to multiprocessors using a parallel genetic algorithm. J Parallel Distrib Comput 1997;47(1):58–77.